IEEE Photonics Journal
An IEEE Photonics Society Publication

Open Access

Study of Pulse Formation in an EDFL Under a Large Dispersion Variation Hybridly Mode-Locked by Graphene and Nonlinear Polarization Rotation

Volume 13, Number 2, April 2021

David Steinberg
Juan Diego Zapata
Lucia A. M. Saito
Eunezio A. Thoroh de Souza

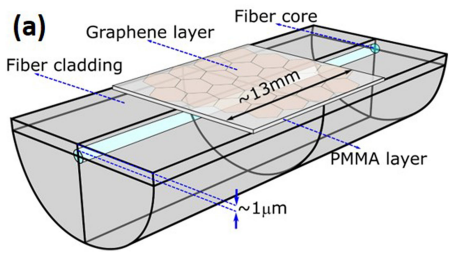

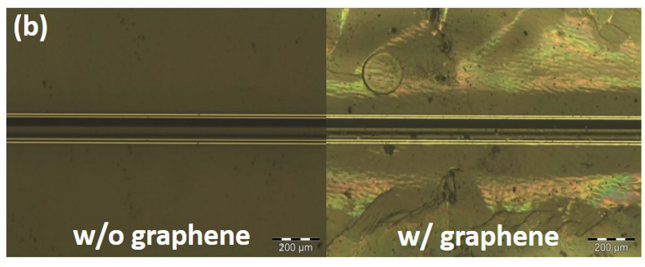

DOI: 10.1109/JPHOT.2021.3061519

Study of Pulse Formation in an EDFL Under a Large Dispersion Variation Hybridly Mode-Locked by Graphene and Nonlinear Polarization Rotation

David Steinberg,[1] **Juan Diego Zapata**,[2] **Lucia A. M. Saito**,[1] **and Eunezio A. Thoroh de Souza**[1]

[1]MackGraphe–Graphene, Nanomaterials and Nanotechnology Research Center, Mackenzie Presbyterian University, São Paulo 896-01302-907, Brazil
[2]Faculty of Engineering, Universidad de Antioquia, Medellin 53-108, Colombia

DOI:10.1109/JPHOT.2021.3061519

Manuscript received November 4, 2020; revised February 17, 2021; accepted February 20, 2021. Date of publication February 26, 2021; date of current version March 12, 2021. Corresponding author: David Steinberg (e-mail: datiolle@hotmail.com).

Abstract: In this work, we present a detailed experimental study of pulse formation mechanism in an EDFL, hybridly mode-locked by use of a CVD monolayer graphene onto a D-shaped optical fiber and nonlinear polarization rotation (NPR), under a large intracavity dispersion influence (up to 100 times) ranging from 12.3 to 1382 m cavity lengths. Analyzing the spectral evolution, temporal and soliton behaviors of the pulse, our results revealed the presence of four laser operating regimes with non-soliton and soliton formation from short to ultralong cavity lengths, all related to graphene/NPR nonlinearities, dispersion and soliton propagation influences.

Index Terms: CVD monolayer graphene, Mode-locked Erbium doped fiber laser, D-shaped optical fiber, short-long-ultralong cavities.

1. Introduction

Mode-locked fiber laser has been one of the efficient technologies for many optical applications, such as communication for optical frequency comb generator and wavelength converter, chemical, physical, and biological procedures, due to their ultrashort pulse generation capacity [1]–[3]. Especially in optical communications, mode-locked Erbium-doped fiber laser (EDFL) based on physical [3] or artificial [4] saturable absorber (SA) has been mostly used as an excellent alternative for generating ultrashort pulses on compact, low-cost fiber system at 1550 nm. In the first class, a nanomaterial is incorporated as SA into the laser cavity to achieve the passive mode-locking condition, depending on only the nonlinear optical response of the nanomaterial. In the past decades, two types of these saturable absorbers have been widely used for ultrashort pulses generation through passive mode-locked lasers: semiconductor saturable absorber mirrors (SESAM) [3] and single-wall carbon nanotubes (SWCNT) [5], [6]. Despite the good properties of these materials, some disadvantages such as infrared narrow-spectrum operation, low damage threshold, expensive fabrication (for SESAM), high nonsaturable losses and their diameter selectivity (for SWCNTs) have been some of the most significant challenges for low-loss mode-locked fiber laser systems in the infrared broadband fiber spectrum.

Graphene is a two-dimensional carbon allotrope nanomaterial consisting of one atom thickness with many important electronic and optical properties [7]. In fact, graphene has been proposed as a promising material for researchers and industry in nanomaterials, nano-electronics, opto-electronics, and photonics areas [8]. Properties such as ultrafast carrier dynamics, broadband absorption, high transparency, and nonlinear optical effects make graphene an ideal polarizer and saturable absorber for broadband optical fiber lasers [8]–[12]. For passive mode-locking, graphene has been widely incorporated as SA into several EDFL configurations by means of well-known light interaction mechanisms (optical fiber tip, taper fiber, D-shaped optical fiber), resulting in remarkable lasers performances with sub-picosecond pulse generation [13]–[24]. In the same platform, new 2D-nanomaterials as topological insulators [25], transition metal dichalcogenides [26]–[28], black phosphorus [29], [30] and other layered materials [31] have also been studied and used for the same propose.

The second class for ultrashort pulse generation in mode-locked fibers lasers is artificial SA, which includes nonlinear polarization rotation (NPR) [4], [32], nonlinear optical loop mirror (NOLM) [4], [33], and nonlinear amplifying loop mirror (NALM) [4], [34] as optical Kerr effect based mode-locking techniques. Among them, NPR has been the most used as effective mechanism for these applications due to the practical implementation and robust automation for high power and automatic pulse generation in fiber lasers [35]. In the same line, NPR has also been widely implemented for assist hybrid mode-locking. Such hybrid mechanism can provide better laser mode-locking performances (shorter pulses, broader bandwidths) followed by high stability and high pulse energy by the combination of artificial [36] and physical [37]–[39] saturable absorbers. In literature, few passively hybrid mode-locked fiber lasers have been most reported incorporating nanomaterials SA [40]–[45].

By using such mechanisms, mode-locked EDFLs have been widely demonstrated and studied at different ranges of cavity lengths, also extended for ultralong range for sensor [46], data transmission [47], and high-energy pulse lasers applications [48], [49], and for investigating the dynamics of pulse generation and propagation as a function of cavity/dispersion parameters. Agrawal *et al*. [50] and Dulling *et al*. [51] were the first groups to experimentally and theoretically determine the pulse propagation behavior in general mode-locked fiber lasers. In the latter, pulses of 100-500 fs were generated and parabolically adjusted in terms of dispersion parameters in a short-length figure eight (F8) EDFL using NALM mechanism [51].

From these works, few studies of EDFLs with similar approaches have been reported in the literature. From an active ultralong EDFL, picosecond pulses were generated at GHz high repetition rate by using an electro-optical modulator, showing remarkable results of the soliton effect in anomalous dispersion laser regime [52]–[54]. Based on passive NPR mode-locking mechanism, the study was experimentally and theoretically demonstrated for a long-ultralong EDFL cavity [55]. However, they obtained a particular relation for long-nanosecond pulses with respect of laser cavity. Subsequently, an EDFL based on a single walled carbon nanotubes (SWCNT) SA was demonstrated by Rosa *et al*., covering from short (8 m) to ultra-long (3500 m) lengths [56]. In this work, H. Rosa *et al*. showed a linear tendency of pulse generation as a function of cavity length from short to long EDFL cavities, and an approximate parabolic behavior soliton pulse from long to ultralong EDFL cavities, very similar to those reported by [50] and [51].

Exploring the nonlinear optical properties of carbon-based materials, several soliton and non-soliton [57]–[60] mode locked EDFLs have been reported using graphene SA [11]–[24]. In one of these works, the pulse behavior was theoretically and experimentally studied in a short-length EDFL based on both graphene nanosheets and NPR, used separately, which also showed its parabolic tendency [61]. In the same line, Zapata *et al* has reported the best mode-locking performance of 150 fs [19] obtained from an EDFL based on hybrid mode-locking mechanism between CVD monolayer graphene onto D-shaped fiber and NPR, focusing the same study on short [19], long and ultra-long cavities [62]. The ultrashort pulse generation with graphene onto D-shaped optical fiber has been an efficient manner to improve the light-graphene interaction through the control of the polarization extinction ratio [11], [19], allowing the easy integration in optical fiber-based devices. As graphene plays the most crucial role in the cavity pulse formation

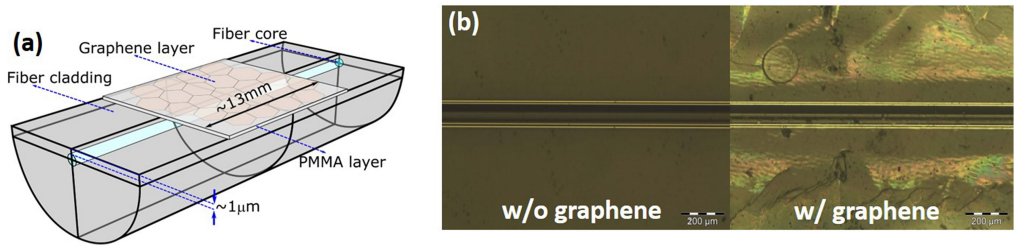

Fig. 1. (a) Illustration of a D-shaped optical fiber with 13 mm of graphene on the side-polished surface. (b) Optical microscopy image of the side-polished of D-shaped optical fiber with (right) and without (left) the graphene/PMMA film.

and the laser gain/loss balance due to its high polarization-dependent loss (PDL) [63] and fast-saturable absorber properties [9] respectively, the material onto D-shaped fiber also contributes to the pulse dynamics and induces the NPR effect inside the laser, resulting in the emergence of hybrid mode-locking mechanism [11], [19]. Because the NPR effect is directly related to the nonlinear phase, accumulated dispersion, fiber length, fiber nonlinearity, and pulse peak power parameters and it is more instable due to environmental fluctuations such as temperature and fiber curvature, the graphene saturable absorption also compensates such issues by stabilizing the laser mode-locking. As a result, the same parabolic behavior as a function of cavity length was observed in both cases in these works.

For the first time, we present an experimental study of pulse formation and propagation in a short, long and ultralong mode-locked EDFL hybridly mode-locked by chemical vapor deposition (CVD) monolayer graphene onto D-shaped optical fiber and NPR mechanisms. We found that the laser mode-locking was highly dependent on managed cavity accumulated dispersion, as expected, which resulted in pulse generation from 160 fs to 3.45 ps with spectrum bandwidth from 33 to 1.67 nm, respectively, at accumulated dispersion range from $+0.061$ to $+23$ ps/nm. According to pulse spectrum evolution, peak power and soliton parameters behaviors as a function of laser cavity length, we identified four operation regimes as divided by (I) short-length stretched to soliton (12.3–14.7 m), (II) soliton short-length (14.7–28.8 m), (III) soliton short-long-length (28.8–209 m) and (IV) soliton long-ultralong length cavities (209–1382 m), all related to graphene/NPR nonlinearity, dispersion, and soliton propagation influences. In contrast to previous reported works [55], [56], [61], [62] we investigated in detail the dynamics of pulse formation in a managed dispersive EDFL severely operating at fundamental repetition rate (single pulse regime) in all cavity lengths, showing for the first time, its non-soliton and soliton pulse parameters under a large dispersion variation influence.

2. Sample Fabrication and Characterization

2.1 Graphene Sample Preparation

A typical CVD process was used to synthesize the monolayer graphene films on copper foils [64]. Fig. 1(a) shows the 13 mm monolayer graphene length, which was transferred from the cooper to the side-polished surface of the D-shaped optical fiber with distance from the core to the polished surface (h) of 1 μm and polishing length of 17 mm by using the wet transfer method, as previously reported by our group [11], [19]. Fig. 1(b) shows the optical microscopy image of the transferred graphene/PMMA film on the polished side of the D-shaped optical fiber using a 10X objective lens.

2.2 Raman Spectroscopy Analysis

A Raman confocal microscope-spectrometer was used to characterize the CVD monolayer graphene sample. Raman spectroscopy measurement was performed with a 532 nm solid-state

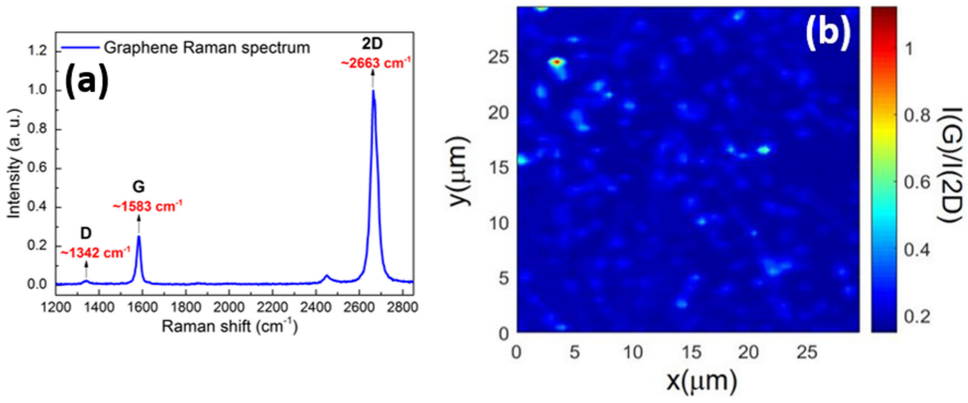

Fig. 2. (a) Raman spectrum of monolayer graphene onto D-shaped optical fiber. (b) Raman mapping showing the IG/I2D intensity ratio from a 30 x 30 μm^2 coverage area on side-polished surface.

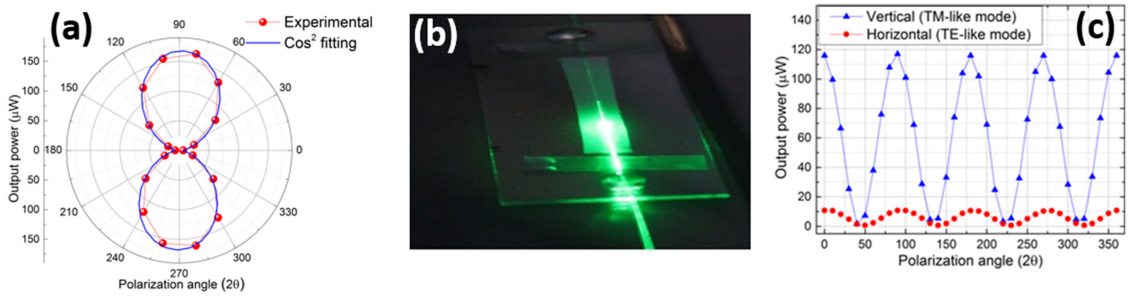

Fig. 3. (a) Transmitted power as a function of polarization angle in polar coordinates for the sample with graphene. (b) Interaction between graphene/PMMA and evanescent field. (c) TE and TM absorption modes in graphene/D-shaped optical fiber. The TE like-mode is stronger absorbed than TM-like mode.

laser with an output power of 3 mW. In Fig. 2(a), it is shown the Raman spectrum of D (1342 cm^{-1}), G (1583 cm^{-1}), and 2D (2663 cm^{-1}) characteristic bands from the transferred monolayer graphene surface [64], [65]. For analyzing the graphene quality along the fiber surface area, we performed a Raman mapping of the I_G/I_{2D} intensity ratio between the G and 2D bands from a 30 μm x 30 μm coverage area on the polished side of the D-shaped optical fiber. In this mapping, 90% of monolayer graphene is observed on image analysis. This percentage is identified in Fig. 2(b) by blue color, where the intensity ratio is $0.25 < I_G/I_{2D} \leq 0.5$. The other areas are composed of the bilayer (yellow color) and multilayer graphene (red to brown tones), which is characteristic of the CVD graphene growth process [64], [65].

2.3 Polarization Setup and TE/TM Modes Analysis

The polarization extinction ratio of the fabricated sample was characterized by using the setup as shown in [11]. The 1550 nm laser beam was collimated with a 20X objective lens. The beam was then vertically polarized through a polarization beam splitter (PBS) and the polarization direction was controlled by the half-wave plate. The polarized beam was coupled to a 1-meter length of single-mode fiber (SMF) through another 20X objective lens and an all-fiber polarization controller was used to minimize the polarization rotation caused by the SMF. After the polarization controller, the SMF was coupled to the fabricated sample and the output power was measured by a power meter. In Fig. 3(a) is shown the interaction curve of the light-evanescent field of D-shaped optical fiber with a core-graphene distance of 1 μm and a graphene length of 13 mm. No

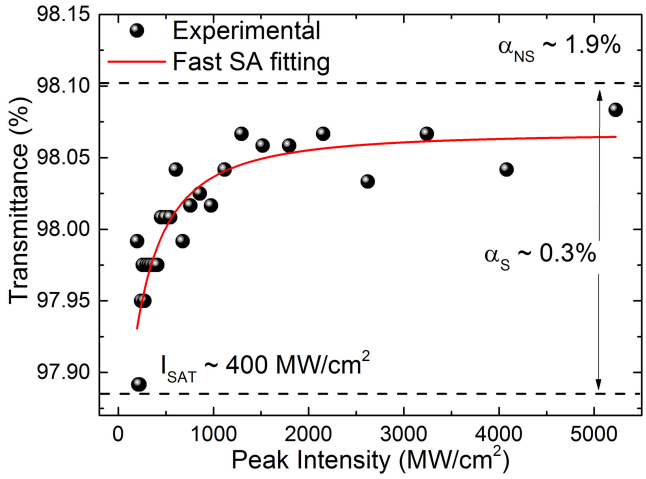

Fig. 4. Saturation absorption curve of CVD monolayer graphene obtained from Z-scan measurement.

polarization-dependent absorption was observed without graphene. The sample exhibited strong induced polarization interaction (red filled circles) with a squared cosine function behavior (blue line curve), and a high insertion loss of ∼9 dB. In polar coordinates, we observed the minimum and maximum power absorption corresponding to the transverse magnetic (TM-like) and transverse electric (TE-like) modes, respectively, relatives to the graphene plane, which resulted in a high polarization relative extinction ratio of 98% [11], [63].

The interaction between the light evanescent field and graphene/PMMA film onto D-shaped optical fiber was observed through the passage of a 532 nm solid-state laser, as shown in Fig. 3(b). From this, we could identify the beginning of the graphene length via the light evanescent field, in which the interaction is stronger due to the high absorption of TE-like mode. As PMMA has a refractive index of 1.49, this significantly improves the light interaction with graphene, allowing the high absorption of TE-like mode and consequently providing high polarization extinction ratio [11], [19], [63]. The high TE-like mode absorption is a fundamental feature for a saturable absorption mechanism in EDFL and fully responsible for the ultrashort pulse generation, which in fact, samples with polarization extinction ratio greater than 85% resulted in pulse duration shorter than 300 fs, as reported in [11], [63]. For this reason, the polarization extinction ratio is essential for the mode-locking mechanism.

The graphene TE-like mode absorption was confirmed by using the same polarization setup. The sample output beam was re-coupled, collimated with a 20X objective lens, and then passed through a polarizer. By adjusting the horizontal and vertical polarization of the polarizer, the output power was measured as a function of the polarization rotation angle of the half-wave plate, determining precisely which modes (TE or TM) exhibited higher absorption with respect of graphene plane. Such results are depicted in Fig. 3(c). As expected, the output horizontal polarization is strongly absorbed compared to vertical polarization, which is in good agreement with our reported works [11], [63].

2.4 Saturable Absorption Measurement

The nonlinear optical properties of the CVD monolayer graphene were investigated using an open aperture Z-scan system with a 1550 nm-femtosecond laser, 150 fs pulse duration and 90 MHz repetition rate. Fig. 4 shows the saturation curve.

From the curve, we could extract values of ∼1.9%, 0.3% and 400 MW/cm^2 of non-saturable absorption, modulation depth, and saturation intensity, respectively, which are in good agreement with some previous reports using monolayer graphene as saturable absorber [11], [15], [18]. The

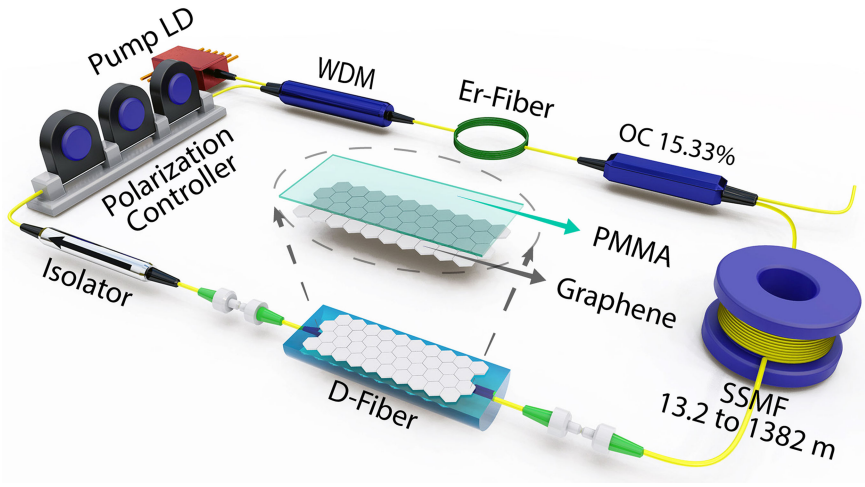

Fig. 5. EDFL setup with graphene SA onto D-shaped optical fiber.

monolayer graphene as a saturable absorber has been considered one of the most important materials for ultrashort pulse generation using passive mode-locking because of its ultrafast relaxation time (∼100 fs), low-intensity saturation, high modulation depth, and low non-saturable absorption properties [7]–[9]. In addition, because of the strong light absorption of the TE parallel component and the longer length of graphene in the D-shaped fiber, there is an increase in the number of electronic transitions at low intensities, which consequently occupies a greater number of electronic states in the material and facilitates the Pauli blocking effect [12]. Therefore, the graphene becomes more efficient as a saturable absorber in the cavity per round trip, resulting in the shorter pulses formation and laser stability improvement [11].

3. Mode-locking Results

3.1 EDFL Setup

The experimental setup is a cavity EDFL with a variable total length from 12.3 to 1382 m, as depicted in Fig. 5. It consists of 2-m length Erbium-doped fiber (-33.8 dB/m absorption coefficient @ 1530 nm and -57 ps/nm/km dispersion coefficient @ 1550 nm), a 980 nm semiconductor pump laser coupled in co-propagating configuration through a 980/1550 nm WDM, a polarization controller, a 50-dB optical isolator and an output coupler of 15.3%. Incorporating the graphene/D-shaped optical fiber SA sample into the EDFL cavity and changing the cavity length, the accumulated dispersion values were between $+0.061$ and $+23$ ps/nm. The spectral and temporal mode-locked pulses were evaluated by using an optical spectrum analyzer and detected by a 12.5 GHz photodetector connected to a 1 GHz sampling oscilloscope. The pulse duration and the output power were measured by using an autocorrelator and a power meter, respectively.

3.2 Output Pulse Duration and Bandwidth As a Function of Cavity Length

In this section, we show the EDFL mode-locking results as a function of cavity length from 12.3 m to 1.38 km, corresponding to the anomalous intracavity-accumulated dispersion range of $+0.061$ to $+23$ ps/nm, and highlighted four main regions of the laser: I (white area), II (green area), III (yellow area) and IV (blue area). All non-self-starting mode-locking regimes were activated by using high pumping power from 80–210 mW and then reduced to 30–60 mW for obtaining the lasers fundamental repetition rate operation (single pulse). The pulse duration (black filled spheres) and bandwidth (red open circles) measurements are shown in Fig. 6(a).

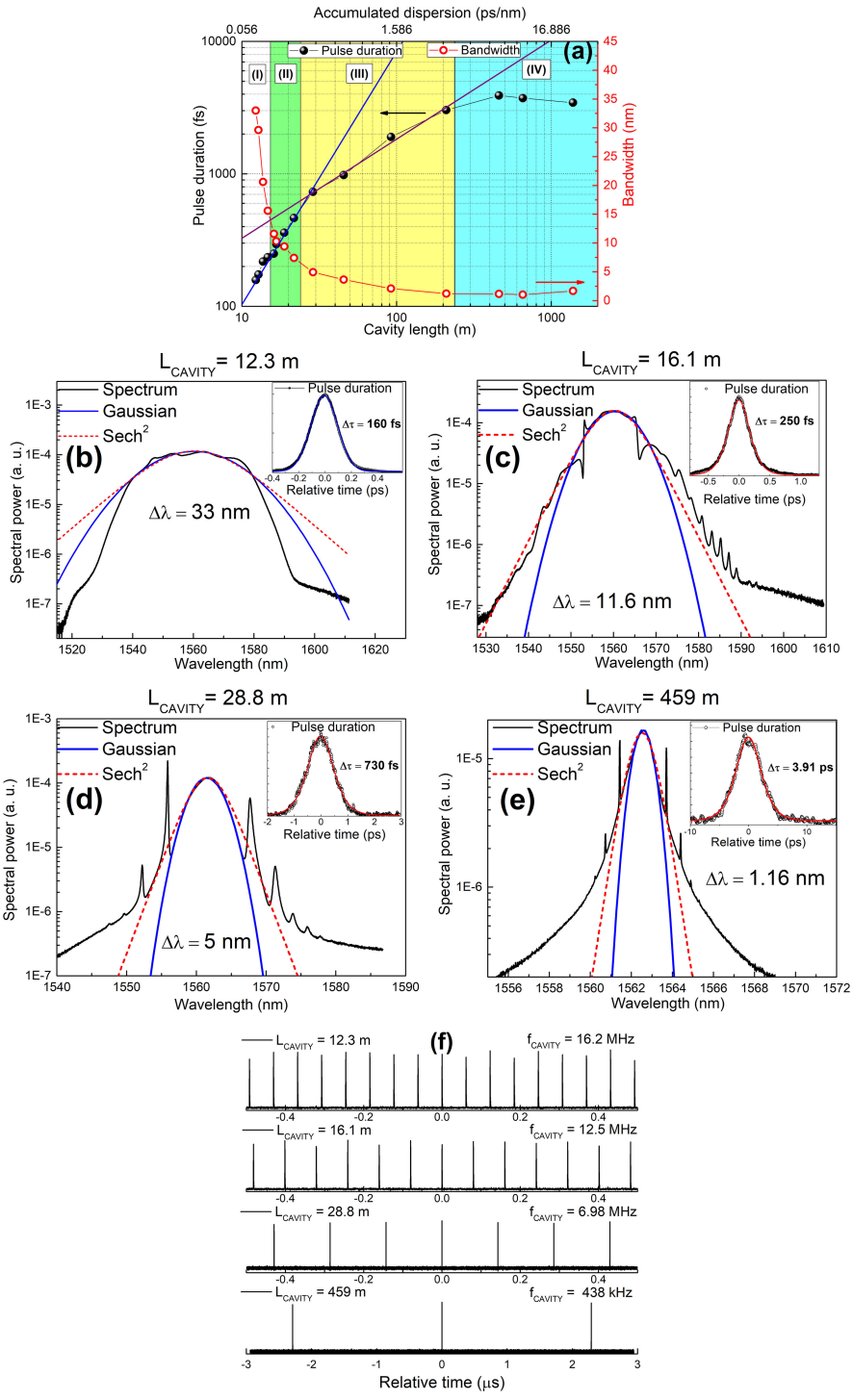

Fig. 6. (a) EDFL output pulse duration (black filled spheres) and bandwidth (red open spheres) as a function of the cavity length/accumulated dispersion showing, as expected, an increase of the pulse duration and a narrowing of its corresponding bandwidth. The blue and purple lines represent the linear tendencies of the region II and III. In (b), (c), (d), (e) and (f), we show the spectrum (fitted by Gaussian and Sech^2) and the pulse durations (inset) of 160 fs for a stretched short cavity (12.3 m), 250 fs for soliton short cavity (16.1 m), 730 fs for soliton short-long cavity and 3.90 ps for soliton long-ultralong cavity (459 m) with their respective fundamental repetition rates.

For the shortest-managed dispersion EDFL of 12.3 m cavity length (+0.061 ps/nm), we measured the broadest bandwidth of 33 nm centered at 1560 nm, showing intrinsic stretching laser behavior [4], [57]–[60], as well-fitted by Gaussian spectral profile, as shown in Fig. 6(b). As result, the corresponding autocorrelation trace was 160 fs (inset - Fig. 6(b)). The mode-locking pulse train was generated at the cavity fundamental repetition rate of 16.3 MHz with measured average output power and calculated intracavity peak power of 0.363 mW and 782 W, respectively. The time-bandwidth product (TBP) of this pulse was 0.642, which is far from the transform-limited value of 0.441 for gaussian pulses. From this point to 14.7 m short lengths (region I), corresponding to the small dispersion regime (+0.061 to +0.102 ps/nm), stretched-like pulses from 160 to 235 fs and bandwidth from 33 to 15.6 nm were generated, respectively.

By slightly increasing the cavity length from the previous region, we entered in the soliton formation zone, as divided into short (region II), short to long (region III) and long to ultralong (region IV) cavity lengths. In the short-long length cavities (16.1–209 m), we measured soliton-like pulses with duration from 250 fs to 3.03 ps (11.6 to 2.1 nm bandwidth), assuming sech^2 profile, and output power from 0.200 to 0.03 mW. The respective intracavity peak powers were 70-370 W, all values near the minimum theoretical value of peak power required to the soliton formation, given by $P_{SOLITON} = 3.11*|D_{AVERAGE}|/(\gamma*\Delta\tau$ (2), where $D_{AVERAGE}$, γ and $\Delta\tau$ are average dispersion, nonlinear coefficient and pulse duration, thus confirming the soliton formation in these regions [50]. In Fig. 6(c) and 6(d) are shown the corresponding spectrum and pulse results obtained for 16.1 and 28.8 m cavity lengths in region II and III, respectively.

Interestingly, both regions II and III showed different behaviors, but with linear tendencies of pulse broadening as a function of cavity length that defined their respective borders. The ratio between the initial and final parameters of the cavity length ($L_{INITIAL}$, L_{FINAL}) and its accumulated dispersion ($D_{INITIAL}$, D_{FINAL}) in the region II was $L_{FINAL}/L_{INITIAL} \sim 2$ and $D_{FINAL}/D_{INITIAL} \sim 3$, thus explaining the sharp tendency ($\Delta\tau = 0.142+1.88*L_{CAVITY}$; Pearson´s coefficient ~0.99) of the curve (blue line) mainly because of the dispersion influence. On the other hand, these parameters were similar in the region III ($L_{FINAL}/L_{INITIAL} \sim 7$; $D_{FINAL}/D_{INITIAL} \sim 10$), however, because of soliton and dispersion influences, the pulse is strongly affected, presenting a smooth tendency ($\Delta\tau = 1.79+0.738*L_{CAVITY}$; Pearson´s coefficient ~ 0.99) (purple line). These experimental curves are in good agreement with those shown in literature for short and long cavities [55], [56], [61], [62].

From 209 to 1382 m cavity lengths (region IV), corresponding to a large dispersion regime (3.41 to 23 ps/nm), the pulse continued to broaden until its saturation at the most extended cavity, as resulted from the significant dispersion influence in this mode-locking regime. For this region, we used an Erbium-doped fiber amplifier (EDFA) to increase the low output power and measured the pulse duration in the autocorrelator with minimum temporal distortion (10-20% for 5-10 dB amplification). For the 459 m long-ultralong EDFL cavity, the laser generated a narrow bandwidth of 1.16 nm (inset - Fig. 6(e)) at a fundamental repetition rate of 438 kHz and output power of 0.027 mW. By linearly amplifying the output power, the measured pulse duration was 3.34 ps and corrected to 3.91 ps (Fig. 6(e)), considering the EDFA calibration. Based on these values, the soliton and intracavity peak powers were calculated to be 4 and 88 W, respectively.

For all laser cavities, we also analyzed the quality of the pulse through the time-bandwidth product (TBP) calculation and directly determined the respective chirp value relative to the gaussian/soliton pulse transformed limit (PTL) for each region. From the calculations, we obtained values of 0.452-0.643 (1.02-1.45 times) for stretched short lasers (region I), 0.357-0.422 (1.13-1.34 times) for soliton short lasers (region II), 0.436-0.493 (1.38-1.57 times) for soliton short-long lasers (region III) and 0.557-0.706 (1.77-2.24 times) for soliton long-ultralong lasers (region IV).

3.3 Output Pulse Spectral Evolution

To verify the mode-locking regimes, we analyzed the spectral evolution obtained for all laser configurations and observed the four mentioned laser regions, as shown in Fig. 7.

At 12.3-14.7 m short lengths (region I), the laser exhibited flat broadband spectra profile, characteristic of stretched laser mode-locking [4], [57]–[60], as the cavity length slightly increases.

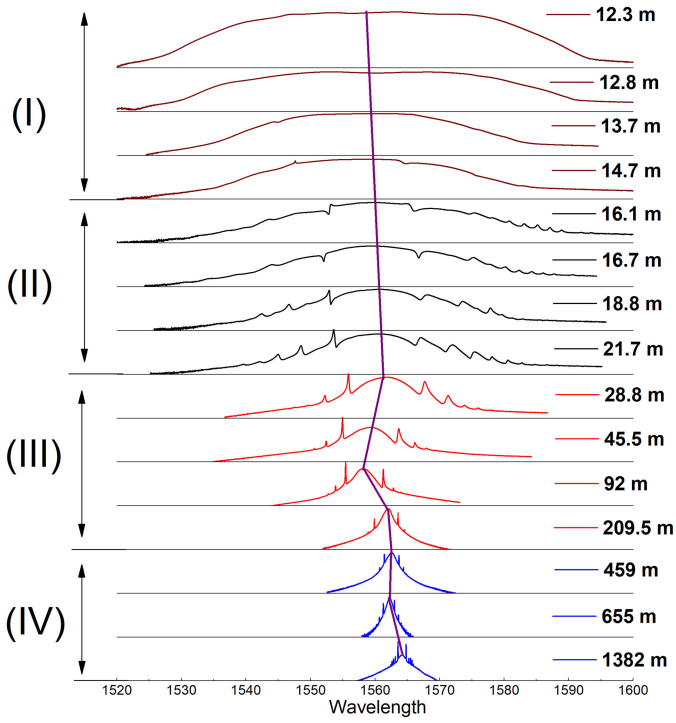

Fig. 7. Spectral evolution from short to ultralong mode-locked EDFL cavities. In addition to narrowing the bandwidth and changing the profile, we observed a shift in the central wavelength, determining four different regimes that depend on the cavity length.

From this point, there is a spectral transition from stretched to soliton regimes (region II) with the appearance of dip-like and Kelly sidebands formation [66]. Because of the small dispersion, the regime is dominated by graphene/NPR nonlinearity because of shorter pulses and broader bandwidths generation but presenting a high chirp level as caused by self-phase modulation (SPM) frequencies excess within the spectrum.

From 28.8 to 209 m (region III), the soliton spectrum profile followed by the emergence of Kelly sidebands is evident, as well as its narrowing due to soliton propagation influence. Comparable to the previous region, the pulse duration (bandwidth) enlarges (narrows) proportionally to the cavity length, which shows a balance between the graphene/NPR nonlinearity and soliton contributions. As we continually increase the cavity length until 1382 m (region IV), soliton behavior is clearly observed as the dominant phenomenon, characterized by long-to-short wavelength spectrum shifting. In this range, the mode-locking performances are constant and spectral/temporal limited by the soliton and large intracavity dispersion effects.

4. Discussions

4.1 Propagation Effect Based on Solitonic Analysis

For analyzing in detail the pulse behavior in the soliton cavities (regions II, III and IV), we plotted the intracavity peak power and fundamental soliton peak power (Fig. 8(a)), the corresponding soliton order (Fig. 8(b)) and the cavity length/soliton period ratio (Fig. 8(c)), all parameters as a function of the cavity length/accumulated dispersion. Based on the spectrum evolution and pulse duration behavior, we also identified different types of solitons in the three cavity regions of the laser.

4.1.1 Short-length Cavities (Region II): In the region II (green area), it consists of broadband soliton lasers (Fig. 7), which generated ultrashort pulses on the femtosecond scale (250-465 fs)

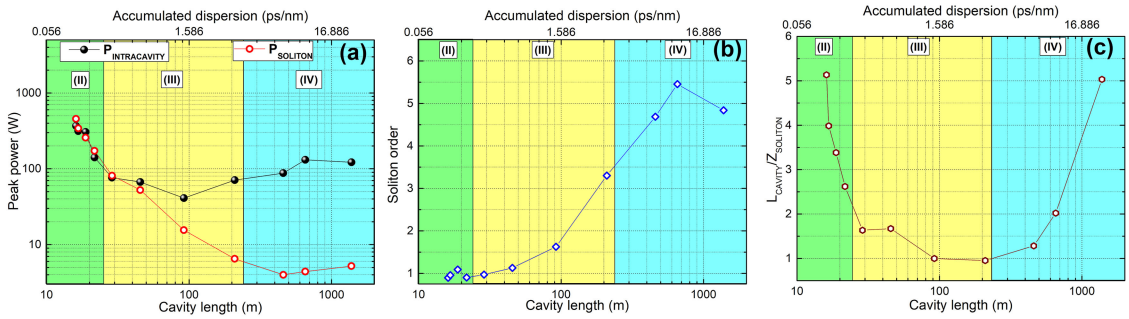

Fig. 8. (a) Intracavity pulse peak (black filled spheres)/soliton powers (red open circle), (b) soliton order, and (c) cavity length/soliton period ratio as a function of the cavity length/accumulated dispersion. The regions II, III, and IV are represented by green, yellow, and blue areas, respectively.

at tens of MHz repetition rate. In this range, the pulse peak power is mainly determined by the pulse duration, mostly derived from SPM and graphene/NPR simultaneous combination at a small dispersion regime. As a result, high peak pulse powers could be easily measured from 140 to 370 W (Fig. 8(a)), values like those obtained by the soliton power calculation, which generated stable fundamental soliton ($N = 1$) in all short-length cavities (Fig. 8(b)).

Another important parameter to be considered in the study of soliton is the soliton period, given by $Z_{SOLITON} = [0.322{*}\pi\ (2){*}c{*}\Delta\tau\ (2)]/[\lambda\ (2){*}D_{AVERAGE}]$ [50]. In Fig. 8(c), because of small dispersion in this regime, we observed that the cavity length is always longer than the soliton period ($L_{CAVITY} > Z_{SOLITON}$), varying from 5 (16.1 m) to 1.5 times (28.8 m). Although these can be significant values in terms of periodic soliton oscillations inside the cavity, this effect is negligible when examining the fundamental soliton, which maintains its temporal profile regardless of soliton length.

4.1.2 Short-long Length Cavities (Region III): From the 28.8 m cavity, there is a transition from short to long cavity laser as well as different types of soliton pulses (yellow area). As we increased the cavity length seven times, the pulse duration quadruplicated, changing from femtosecond to picosecond range, consequently affecting its peak power, soliton order, and soliton period at different levels. In the first case, the pulse starts to present higher intracavity power than its soliton power until reaching its minimum value at 92 m. Despite the large gap between the two powers, the soliton stands in its fundamental state ($N = 1$), but without undergoing any periodic oscillation within the cavities ($L_{CAVITY} \sim Z_{SOLITON}$). Although there is a transition from fundamental to higher-order soliton ($N > 2$) from this point up to 209 m, the pulse changes its spectral/temporal profile throughout its propagation, but within its soliton period. Therefore, except for this latter length, we can consider this region the most stable, in terms of soliton parameters, for generation and propagation of soliton pulses, showing the strong balance between graphene/NPR/SPM nonlinearities and soliton propagation effects.

4.1.3 Long-ultralong Length Cavities (Region IV): By continuously increasing the cavity length from 209 to 1382 m, we achieved the long to the ultralong regime (blue area), in which the laser mode-locking performances are determined by soliton and large dispersion effects. Because of the low repetition rate of these cavities (kHz range) and the pulse broadening, the pulse intracavity peak power is almost 2 orders of magnitude its soliton power at the long-ultralong range, becoming very unstable as a higher-order soliton ($N > 2$). In the same direction, the estimated number of periodic oscillations within these cavities potentially grows ($L_{CAVITY} > Z_{SOLITON}$) and reaches a maximum value of 5 at 1382 m cavity, almost the same value than that observed in the shortest soliton laser cavity (16.1 m). Therefore, the simultaneous combination of these two parameters directly reflects on soliton instability inside these cavities and, consequently, on difficulty level for obtaining the laser single pulse regime.

TABLE 1
Experimental Pulse Formation Studies From All Reported Mode-Locked EDFLs Ranging From Short to Ultralong Cavity Lengths

Ref.	Saturable absorber			Laser cavity length range			Study and analysis
	Artificial	Physical	Hybrid	Short	Long	Ultralong	Experimental
[51]	NALM	------	------	X	------	------	$\Delta\tau_P$ x D
[55]	NPR	------	------	------	X	X	$\Delta\tau_P$ x L E_P x L
[56]	------	CNT	------	X	X	X	$\Delta\tau_P$ x L $\Delta\tau_P$ x D
[61]	NPR	Graphene nanosheets	------	X	------	------	$\Delta\tau_P$ x L
[11] [19]	NPR	CVD Graphene	X	X	------	------	$\Delta\tau_P$ x L
[62]	NPR	CVD Graphene	X	X	X	X	$\Delta\tau_P$ x L
This work	**NPR**	**CVD Graphene**	**X**	**X**	**X**	**X**	**$\Delta\tau_P$ x L** **P_{SOL} x L** **Z_{SOL} x L** **N_{SOL} x L**

Table 1 shows the EDFL reported works, considering the (1) saturable absorber type (artificial, physical or hybrid) used in the laser, (2) cavity length range (short, long or ultralong) and (3) experimental study/analysis of each work.

All references incorporated different types of saturable absorbers (artificial or physical) as a unique mechanism for generating the mode-locking regime, which unlike this work, the hybrid mechanism was carefully analyzed in short, long and ultralong cavities. Also, all cited works presented only the pulse duration behavior as a function of cavity length/dispersion. By rigorously measuring the mode-locking regime of all EDFL cavities at the fundamental repetition rate (single pulse operation), this experiment became more accurate, so that we could expand the same study and explore important pulse parameters in terms of peak power and soliton propagation. Based on these approaches, we believe this is the first and unique experimental study of the dynamics of pulse formation and propagation in an EDFL hybridly mode-locked by CVD monolayer graphene and NPR mechanisms ranging from short to ultralong cavities.

5. Conclusion

In summary, we presented a detailed experimental study of soliton and non-soliton pulse behavior at short, long, and ultralong mode-locked EDFL cavities based on CVD monolayer graphene onto D-shaped optical fiber and nonlinear polarization rotation hybrid mechanism. By changing the laser cavity length from 12.3 m to 1.38 km, we could obtain pulses from 160 fs to 3.45 ps. The laser spectra evolution, pulse peak power and temporal width behaviors showed the existence of four operation regions located at small, medium, and large dispersion ranges: stretched and soliton short cavities, soliton short-long cavities, and soliton long-ultralong cavities. At soliton short cavities (14.7–28.8 m), the laser mode-locking performance is mainly attributed to graphene/NPR nonlinearity and self-phase modulation, generating sub-picosecond pulses, broad bandwidths, and high pulse peak power; at short-long cavities (28.8–209 m), the laser performance, as well as its intracavity peak power decreases until a minimum value under both graphene/NPR nonlinearity and dispersion influences; at long-ultralong cavities (209–1382 m), the pulse dynamics is entirely

governed by dispersion and soliton propagation effects. Also, we could estimate the fundamental soliton formation as characterized by the pulse peak power stabilization promoted by SPM and graphene/NPR for short-to-long length cavities and higher-order soliton formation due to high pulse peak power instabilities and dispersion parameters for long-to-ultralong length cavities.

Acknowledgment

The authors wish to thank the Fundação de Amparo à Pesquisa do Estado de São Paulo (FAPESP) (SPEC 2012/50259-8, 2015/11779-4, 2016/25836-2), Coordenação de Aperfeiçoamento de Pessoal de Nível Superior (CAPES) (1716664; PrInt processo n° 88887.310281/2018-00), Full time University of Antioquia, Electronic department First Project Acta (n° 2018-22673), projeto:G8 - 2020 3906 Universidad de Antioquia y Ruta N, and Fundo Mackenzie de Pesquisa (MackPesquisa).

References

[1] F. Meng and J. M. Dudley, "Toward a self-driving ultrafast fiber laser," *Light Sci. Appl.*, vol. 9, 2020, Art. no. 26.
[2] W. Shi, Q. Fang, X. Zhu, R. A. Norwood, and N. Peyghambarian, "Fiber lasers and their applications," *App. Opt.*, vol. 53, no. 28, pp. 6554–6568, 2014.
[3] U. Keller, "Recent developments in compact ultrafast lasers," *Nature*, vol. 424, pp. 831–838, 2003.
[4] L. E. Nelson, D. J. Jones, K. Tamura, H. A. Haus, and E. P. Ippen, "Ultrashort-pulse fiber ring lasers," *Appl. Phys. B*, vol. 65, pp. 277–294, 1997.
[5] D. Li *et al.*, "Wavelength and pulse duration tunable ultrafast fiber laser mode-locked with carbon nanotubes," *Sci. Rep.*, vol. 8, 2018, Art. no. 2738.
[6] H. G. Rosa and E. A. De Souza, "Bandwidth optimization of a carbon nanotubes mode-locked erbium-doped fiber laser," *Opt. Fiber Technol.*, vol. 18, pp. 59–62, 2012.
[7] A. H. Castro Neto, F. Guinea, N. M. R. Peres, K. S. Novoselov, and A. K. Geim, "The electronic properties of graphene," *Rev. Mod. Phys.*, vol. 81, no. 1, pp. 109–162, 2009.
[8] F. Bonaccorso, Z. Sun, T. Hasan, and A. C. Ferrari, "Graphene photonics and optoelectronics," *Nat. Photon.*, vol. 4, pp. 611–622, 2010.
[9] Q. Bao and K. P. Loh, "Graphene photonics, plasmonics, and broadband optoelectronic devices," *ACS Nano*, vol. 6, pp. 3677–3694, 2012.
[10] M. Baudisch *et al.*, "Ultrafast nonlinear optical response of dirac fermions in graphene," *Nat. Commun.*, vol. 9, 2018, Art. no. 1018.
[11] J. D. Zapata, D. Steinberg, L. A. M. Saito, R. E. P. de Oliveira, A. M. Cárdenas, and E. A. Thoroh de Souza, "Efficient graphene saturable absorbers on D-shaped optical fiber for ultrashort pulse generation," *Sci. Rep.*, vol. 6, 2016, Art. no. 20644.
[12] F. Zhang, S. Han, Y. Liu, Z. Wang, and X. Xu, "Dependence of the saturable absorption of graphene upon excitation photon energy," *Appl. Phys. Lett.*, vol. 106, no. 9, pp. 1–6, 2015.
[13] T. Hasan *et al.*, "Nanotube–polymer composites for ultrafast photonics," *Adv. Mater.*, vol. 21, pp. 3874–3899, 2009.
[14] Q. Bao *et al.*, "Atomic layer graphene as saturable absorber for ultrafast pulsed laser," *Adv. Funct. Mater.*, vol. 19, no. 19, pp. 3077–3083, 2009.
[15] Q. Bao *et al.*, "Monolayer graphene as a saturable absorber in a mode-locked laser," *Nano. Res.*, vol. 4, no. 3, pp. 297–307, 2011.
[16] G. Sobon and J. Sotor, "Recent advances in ultrafast fiber lasers Mode-locked with Graphene- based Saturable absorbers," *Curr. Nanosci.*, vol. 12, no. 3, pp. 291–298, 2016.
[17] K. Chen *et al.*, "Graphene photonic crystal fibre with strong and tunable light–matter interaction," *Nature*, vol. 13, pp. 754–759, 2019.
[18] N. H. Park, H. Jeong, S. Y. Choi, M. H. Kim, F. Rotermund, and D.-I. Yeom, "Monolayer graphene saturable absorbers with strongly enhanced evanescent-field interaction for ultrafast fiber laser mode-locking," *Opt. Exp.*, vol. 23, no. 15, pp. 19806–19812, 2015.
[19] J. D. Zapata, L. A. M. Saito, A. M. Cárdenas, and E. A. Thoroh de Souza, "Sub-150 fs mode-locked erbium doped fiber laser based on monolayer graphene on a D-shaped optical fiber," in *Proc. Conf. Lasers Electro-Opt. (CLEO)*, 2016, presentation number: JTu5A.71.
[20] D. Steinberg, J. D. Zapata, E. A. Thoroh de Souza, and L. A. M. Saito, "Mechanically exfoliated graphite onto D-shaped optical fiber for femtosecond mode-locked Erbium-doped fiber laser," *J. Lightw. Technol.*, vol. 36, no. 10, pp. 1868–1874, 2018.
[21] D. Steinberg *et al.*, "Graphene oxide and reduced graphene oxide as saturable absorbers onto D-shaped fibers for sub-200 fs EDFL modelocking," *Opt. Mater. Exp.*, vol. 8, no. 1, pp. 144–156, 2018.
[22] H. G. Rosa, J. C. V. Gomes, and E. A. Thoroh de Souza, "Transfer of an exfoliated monolayer graphene flake onto an optical fiber end face for erbium-doped fiber laser mode-locking," *2D Mater.*, vol. 2, no. 3, 2015, Art. no. 031001.
[23] H. G. Rosa *et al.*, "Raman mapping characterization of all-fiber CVD monolayer graphene saturable absorbers for erbium-doped fiber laser mode locking," *J. Lightw. Technol.*, vol. 33, no. 19, pp. 4118–4123, 2015.

[24] J. Tarka *et al.*, "Power scaling of an All-PM fiber er-doped mode-locked laser based on graphene saturable absorber," *IEEE J. Sel. Topics Quantum Electron.*, vol. 23, no. 1, pp. 60–65, 2017.
[25] W. Liu *et al.*, "70-fs mode-locked erbium-doped fiber laser with topological insulator," *Sci. Rep.*, vol. 6, pp. 19997, 2016.
[26] R. Woodward, I. Kelleher, and J. R. Edmund, "2D saturable absorbers for fibre lasers," *Appl. Sci.*, vol. 5, no. 4, pp. 1440–1456, 2015.
[27] E. J. Aiub, D. Steinberg, E. A. Thoroh De Souza, and L. A. M. Saito, "200-fs mode-locked Erbium-doped fiber laser by using mechanically exfoliated MoS_2 saturable absorber onto D-shaped optical fiber," *Opt. Exp.*, vol. 25, no. 9, pp. 10546–10552, 2017.
[28] D. Steinberg, J. D. Zapata, E. A. Thoroh de Souza, and L. A. M. Saito, "Mechanically exfoliated rhenium disulfide onto D-shaped optical fiber for sub-300 fs EDFL mode-locking," in *Proc. Conf. Lasers Electro-Opt. (CLEO)*, 2018, presentation number: SM2N.3.
[29] S. B. Lu *et al.*, "Broadband nonlinear optical response in multi-layer black phosphorus: An emerging infrared and mid-infrared optical material," *Opt. Exp.*, vol. 23, no. 9, pp. 11183–11194, 2015.
[30] R. M. Gerosa *et al.*, "Liquid phase exfoliated black phosphorus and reduced graphene oxide polymer-based saturable absorbers fabrication using the droplet method for mode-locking applications," *J. Opt. Laser Tech.*, vol. 106, pp. 107–112, 2018.
[31] T. Jiang, "Ultrafast fiber lasers mode-locked by two-dimensional materials: Review and prospect," *Photon. Res.*, vol. 8, no. 1, pp. 70–90, 2020.
[32] X. Shang *et al.*, "170 mW-level mode-locked Er-doped fiber laser oscillator based on nonlinear polarization rotation," *Appl. Phys. B: Lasers Opt.*, vol. 125, no. 10, pp. 1–7, 2020.
[33] H. Ahmad, M. H. M. Ahmed, and M. Z. Samion, "Generation of mode-locked noise-like pulses in double-clad Tm-doped fibre laser with nonlinear optical loop mirror," *J. Modern Opt.*, vol. 67, no. 2, pp. 146–152, 2019.
[34] D. Deng, H. Zhang, Q. Gong, L. He, D. Li, and M. Gong, "Energy scalability of the dissipative soliton in an all-normal-dispersion fiber laser with nonlinear amplifying loop mirror," *Opt. Laser Technol.*, vol. 125, 2020, Art. no. 106010.
[35] G. Pu, L. Zhang, W. Hu, and L. Yi, "Automatic mode-locking fiber lasers: Progress and perspectives," *Sci. China Inf. Sci.*, vol. 63, no. 6, 2020, Art. no. 160404.
[36] Z. Dong *et al.*, "Er-doped mode-locked fiber lasers based on nonlinear polarization rotation and nonlinear multimode interference," *Opt. Laser Technol.*, vol. 130, 2020, Art. no. 106337.
[37] I. Hernandez-Romano, J. Davila-Rodriguez, D. Mandridis, J. J. Sanchez-Mondragon, D. A. May-Arrioja, and P. J. Delfyett, "Hybrid mode locked fiber laser using a PDMS/SWCNT composite operating at 4 GHz," *J. Lightw. Technol.*, vol. 29, pp. 3237–3242, 2011.
[38] H. Hu, X. Zhang, W. Li, and N. K. Dutta, "Hybrid mode-locked fiber ring laser using graphene and charcoal nanoparticles as saturable absorbers," *Proc. SPIE 9836, Micro Nanotechnol. Sensors, Syst., Appl. VIII*, 2016, presentation number: 983630.
[39] T. Hirooka, K. Tokuhira, M. Yoshida, and M. Nakazawa, "440 fs, 9.2 GHz regeneratively mode-locked erbium fiber laser with a combination of higher-order solitons and a SESAM saturable absorber," *Opt. Exp.*, vol. 24, no. 21, pp. 24255–24264, 2016.
[40] S. Kim *et al.*, "Hybrid mode-locked Er-doped fiber femtosecond oscillator with 156 mW output power," *Opt. Exp.*, vol. 20, no. 14, pp. 15054–15060, 2012.
[41] J. Boguslawski *et al.*, "Investigation on pulse shaping in fiber laser hybrid mode-locked by Sb_2Te_3 saturable absorber," *Opt. Exp.*, vol. 23, no. 22, 2015, Art. no. 29014.
[42] M. A. Chernysheva *et al.*, "Higher-order soliton generation in hybrid mode-locked thulium-doped fiber ring laser," *IEEE J. Sel. Topics Quantum Electron.*, vol. 20, no. 5, pp. 425–432, Sep./Oct. 2014.
[43] D. S. Chernykh *et al.*, "Hybrid mode-locked erbium-doped all-fiber soliton laser with a distributed polarizer," *Appl. Opt.*, vol. 53, no. 29, pp. 6654–6662, 2014.
[44] T.-H. Chen *et al.*, "Incorporating MoS_2 saturable absorption with nonlinear polarization rotation for stabilized mode-locking fibre lasers," *Laser Phys. Lett.*, vol. 15, 2018, Art. no. 075102.
[45] X. Wu, L. Yang, H. Zhang, H. Yang, H. Wei, and Y. Li, "Hybrid mode-locked Er-fiber oscillator with a wide repetition rate stabilization range," *Appl. Opt.*, vol. 54, no. 7, pp. 1681–1687, 2015.
[46] V. De Miguel-Soto, D. Leandro, and M. Lopez-Amo, "Ultra-long (290 km) remote interrogation sensor network based on a random distributed feedback fiber laser," *Opt. Exp.*, vol. 26, no. 21, pp. 27189–27200, 2018.
[47] F. Gallazzi, G. Rizzelli, M. A. Iqbal, M. Tan, P. Harper, and J. D. A.-Castañón, "Performance optimization in ultra-long raman laser amplified 10×30 GBaud DP-QPSK transmission: Balancing RIN and ASE noise," *Opt. Exp.*, vol. 25, no. 18, pp. 21454–21459, 2017.
[48] B. N. Nyushkov *et al.*, "Generation of 1.7-μJ pulses at 1.55 μm by a self-modelocked all-fiber laser with a kilometers-long linear-ring cavity," *Laser Phys. Lett*, vol. 7, no. 9, pp. 661–665, 2010.
[49] B. N. Nyushkov *et al.*, "Gamma-shaped long-cavity normal-dispersion modelocked Er-fiber laser for sub-nanosecond high-energy pulsed generation," *Laser Phys. Lett*, vol. 9, no. 1, pp. 59–67, 2010.
[50] G. P. Agrawal, *Nonlinear Fiber Optics*, 5th ed. Berlin, Germany: Springer, 2013.
[51] M. L. Dennis and I. N. Dulling, III, "Role of dispersion in limiting pulse width in fiber lasers," *Appl. Phys. Lett.*, vol. 62, no. 23, pp. 2911–2913, 1993.
[52] L. A. M. Saito, M. A. Romero, and E. A. de Souza, "48.8 km ultralong erbium fiber laser in active mode-locking operation," *Opt. Rev.*, vol. 17, no. 4, pp. 385–387, 2010.
[53] L. A. M. Saito and E. A. Thoroh de Souza, "A comparison between in-field and in-laboratory 50 km ultralong erbium doped fiber lasers actively mode-locked," *Opt. Exp.*, vol. 20, no. 15, pp. 17001–17009, 2012.
[54] L. A. M. Saito and E. A. Thoroh de Souza, "Identifying the mechanisms of pulse formation and evolution in actively mode-locked erbium fiber lasers with meters and kilometers-long," *Opt. Laser Technol.*, vol. 71, pp. 16–21, 2015.
[55] N. Li *et al.*, "Cavity length optimization for high energy pulse generation in a long cavity passively mode-locked all fiber ring laser," *Appl. Opt.*, vol. 51, no. 17, pp. 3726–3730, 2012.

[56] H. G. Rosa and E. A. Thoroh de Souza, "Pulse duration propagation in dispersion-managed ultralong erbium-doped fiber lasers mode-locked by carbon nanotubes," *Opt. Lett.*, vol. 37, no. 24, pp. 5211–5213, 2012.
[57] K. Tamura, L. E. Nelson, H. A. Haus, and E. P. Ippen, "Soliton versus nonsoliton operation of fiber ring lasers," *Appl. Phys. Lett.*, vol. 62, no. 2, pp. 149–151, 1994.
[58] W. L. Li, Y. C. Kong, G. W. Chen, and H. R. Yang State, "Coexistence of conventional solitons and stretched pulses in a fiber laser mode-locked by carbon nanotubes," *Laser Phys.*, vol. 25, no. 4, pp. 1–5, 2015.
[59] J. Sotor, I. Pasternak, A. Krajewska W. Strupinski, and G. Sobon, "Sub-90 fs a stretched-pulse mode-locked fiber laser based on a graphene saturable absorber," *Opt. Exp.*, vol. 23, no. 21, pp. 27503–27508, 2015.
[60] W. He, M. Pang, C. R. Menyuk, and P. St. J. Russell, "Sub-100-fs 1.87 GHz mode-locked fiber laser using stretched-soliton effects," *Optica,* vol. 3, no. 12, pp. 1366–1372, 2016.
[61] C. Y. Yang, Y. H. Lin, Y. C. Chi, C. L. Wu, J. Y. Lo, and G. R. Lin, "Pulse-width saturation and kelly-sideband shift in a graphene-nanosheet mode-locked fiber laser with weak negative dispersion," *Mater. Chem. Phys.*, vol. 3, no. 4, 2015, Art. no. 044016.
[62] J. D. Zapata, D. Steinberg, L. A. M. Saito, and E. A. Thoroh de Souza, "Ultrashort pulse generation performance in short and ultralong EDFL cavities using CVD monolayer graphene," in *Proc. Latin Amer. Opt. Photon. Conf.*, 2018, presentation number: W2D.2.
[63] R. E. P. De Oliveira and C. J. S. De Matos, "Graphene based waveguide polarizers: In-depth physical analysis and relevant parameters," *Sci. Rep.*, vol. 5, 2015, Art. no.16949.
[64] G. C. Mastrapa, M. E. H. Maia da Costa, D. G. Larrude, and F. L. Freire, "Synthesis and characterization of graphene layers prepared by low-pressure chemical vapor deposition using triphenylphosphine as precursor," *Phys. Rev. Appl.*, vol. 166, pp. 37–41, 2015.
[65] L. M. Malard, M. A. Pimenta, G. Dresselhaus, and M. S. Dresselhaus, "Raman spectroscopy in graphene," *Phys. Rep.*, vol. 473, no. 5/6, pp. 51–47, 2009.
[66] M. L. Dennis and I. N. Duling, III, "Experimental study of sideband generation in femtosecond fiber lasers," *IEEE J. Quantum Electron.*, vol. 30, no. 6, pp. 1469–1477, 1994.